◆ Human Brain Mapping 36:1937–1950 (2015) ◆

# Resting State Functional Connectivity of the Subthalamic Nucleus in Parkinson's Disease Assessed Using Arterial Spin-Labeled Perfusion fMRI

**María A. Fernández-Seara,[1,2]* Elisa Mengual,[2,3] Marta Vidorreta,[1] Gabriel Castellanos,[1] Jaione Irigoyen,[1] Elena Erro,[4] and María A. Pastor[1,2]**

[1]*Neuroimaging Laboratory, Division of Neuroscience, Center for Applied Medical Research (CIMA), University of Navarra, Pamplona, Spain*
[2]*CIBERNED, Centro de Investigación Biomédica en Red de Enfermedades Neurodegenerativas, Instituto de Salud Carlos III, Spain*
[3]*Department of Anatomy, Medical School, University of Navarra, Pamplona, Spain*
[4]*Neurology Department, Navarra Hospital Complex, Pamplona, Spain*

**Abstract:** Neurophysiological changes within the cortico-basal ganglia-thalamocortical circuits appear to be a characteristic of Parkinson's disease (PD) pathophysiology. The subthalamic nucleus (STN) is one of the basal ganglia components showing pathological neural activity patterns in PD. In this study, perfusion imaging data, acquired noninvasively using arterial spin-labeled (ASL) perfusion MRI, were used to assess the resting state functional connectivity (FC) of the STN in 24 early-to-moderate PD patients and 34 age-matched healthy controls, to determine whether altered FC in the very low frequency range of the perfusion time signal occurs as a result of the disease. Our results showed that the healthy STN was functionally connected with other nuclei of the basal ganglia and the thalamus, as well as with discrete cortical areas including the insular cortex and the hippocampus. In PD patients, connectivity of the STN was increased with two cortical areas involved in motor and cognitive processes. These findings suggest that hyperconnectivity of the STN could underlie some of the motor and cognitive deficits often present even at early stages of the disease. The FC measures provided good discrimination between controls and patients, suggesting that ASL-derived FC metrics could be a putative PD biomarker. *Hum Brain Mapp 36:1937–1950, 2015.* 

**Key words:** Parkinson's disease; subthalamic nucleus; functional connectivity; arterial spin labeling; perfusion MRI

Additional Supporting Information may be found in the online version of this article.

Contract grant sponsor: The Spanish Ministry of Science and Innovation; Contract grant number: SAF2011–29344 and RYC-2010-07161; Contract grant sponsor: CIBERNED.

*Correspondence to: María A. Fernández-Seara, Center for Applied Medical Research, University of Navarra, Pio XII, 55, 31008 Pamplona, Spain. E-mail: mfseara@unav.es



The authors declare no conflict of interest.

Received for publication 4 June 2014; Revised 2 December 2014; Accepted 13 January 2015.

DOI: 10.1002/hbm.22747

Published online 30 January 2015 in Wiley Online Library (wileyonlinelibrary.com).

## INTRODUCTION

Parkinson's disease (PD) is a neurodegenerative disease characterized by the loss of dopaminergic neurons mainly in the substantia nigra (SN) pars compacta, with the consequent dopamine depletion in the striatum and functional impairment of the parallel cortico-basal ganglia–thalamocortical circuits.

The subthalamic nucleus (STN) is a key component of the basal ganglia that is activated either via a disynaptic disinhibitory pathway from the striatum, the indirect pathway, or via a direct excitatory cortico-subthalamic pathway, the hyperdirect pathway [Nambu et al., 2002], facilitating the inhibitory output of the basal ganglia to the thalamus.

The STN is one of the preferred targets in deep brain stimulation (DBS) treatment of PD patients, with greater clinical benefits than those obtained by stimulating other sites [Krack et al., 2000; Odekerken et al., 2013; Volkmann et al., 2004]. However, despite the significant experience accumulated on DBS in the past years, the mechanisms by which this surgical therapy improves parkinsonian symptoms are not yet fully elucidated [Chiken and Nambu, 2014]. A broader knowledge of the functional networks involving the STN in both the healthy and parkinsonian brain will greatly contribute to a deeper understanding of this therapeutic strategy.

Resting state functional connectivity MRI (fcMRI) allows the noninvasive characterization of functional networks, through the analysis of temporal correlations in the fMRI signal. This technique has been previously used in a number of studies to evaluate functional connectivity (FC) of the basal ganglia in PD [Hacker et al., 2012; Helmich et al., 2010; Kwak et al., 2010; Luo et al., 2014; Seibert et al., 2012]. However, to date, only two studies have examined the FC of the STN, one in healthy subjects [Brunenberg et al., 2012] and another one in PD patients [Baudrexel et al., 2011]. A third study has evaluated the effects of DBS on the effective connectivity in the resting motor network including the STN [Kahan et al., 2014]. In their study, Baudrexel et al. observed hyperconnectivity of the STN with cortical motor areas associated with PD, while Kahan et al. reported a reduction in the STN effective connectivity, induced by DBS. These findings are consistent with the abnormal synchronicity in basal ganglia–thalamo-cortical networks, observed using invasive and noninvasive electrophysiological techniques [for review, see Hammond et al., 2007; Timmermann et al., 2007].

The fcMRI technique has been mainly applied to fMRI signals acquired using imaging sequences sensitive to blood oxygen level-dependent (BOLD) contrast [Auer, 2008]. More recently, however, FC has been evaluated using the perfusion signal sampled with arterial spin-labeled (ASL) perfusion fMRI [Fernandez-Seara et al., 2011; Viviani et al., 2011]. ASL uses electromagnetically labeled arterial blood water as an endogenous tracer for noninvasive quantitative measurements of cerebral perfusion [Detre et al., 1992; Williams et al., 1992]. ASL in combination with a single-shot readout technique can be used to acquire time-resolved perfusion data. Due to the tight coupling between regional perfusion and neural activity [Raichle, 1998], fluctuations in the perfusion signal will reflect changes in the underlying brain activity. In the absence of any experimental task, the perfusion power spectrum is essentially flat as opposed to the BOLD power spectrum that shows increased noise power at low frequencies [Aguirre et al., 2002]. Therefore, ASL might provide a better characterization of low frequency fluctuations than BOLD [Dai et al., 2012]. In addition, recent work has shown that ASL fcMRI has statistical power and reproducibility comparable to that of BOLD fcMRI [Vidorreta et al., 2012, 2014].

In this work, perfusion-based fcMRI has been used to study whole-brain FC of the STN in healthy controls and PD patients, using a seed-to-voxel approach. Using the seed-based method, the signal time-series of the STN was cross-correlated with the time-series of all brain voxels, to generate a FC map. We hypothesized that FC of the STN with other structures of the cortico-basal ganglia–thalamocortical circuits would be increased in PD. In addition, we used receiver operating characteristic (ROC) analysis techniques to evaluate the ability of the FC measures to discriminate PD subjects from controls.

**TABLE I. Demographic and clinical characteristics of the study groups**

| | Controls | Patients |
|---|---|---|
| N (female:male) | 34 (12:22) | 24 (7:17) |
| Age, years | 63.5 (6.6) | 63.4 (6.7) |
| UPDRS III ON | | 12.4 (5.4) |
| Disease duration, years | | 5.7 (3.3) |
| Hoehn &Yahr stage ON | | 1.83 (0.38) |
| Initially affected body side [Right:Left] | | 14:10 |
| MMSE score ON | | 28.5 (1.7) |
| LEDD, mg | | 626.5 (371.2) |

Values are given as mean (SD). SD: standard deviation; LEDD: levodopa equivalent daily dose.

## MATERIALS AND METHODS

### Subjects

This study was approved by the Ethics Research Committee of the University of Navarra and all the subjects signed a written informed consent prior to inclusion. General exclusion criteria for MRI scanning were applied (such as metal implants, pacemakers, and claustrophobia). All subjects were right-handed as measured by the Edinburgh Inventory [Oldfield, 1971]. Detailed demographic and clinical data of the subjects are presented in Table I.

## Patients

Twenty-four PD patients were included in the study. The patients had been diagnosed with idiopathic PD by a neurologist specialized in movement disorders, according to the United Kingdom Parkinson's Disease Society Brain Bank criteria [Hughes et al., 1992]. Exclusion criteria were history of other neurological or psychiatric diseases, moderate-severe head tremor, dyskinesias, and cognitive impairment (Mini Mental State Examination [MMSE] < 25/30, [Folstein et al., 1975]). Patients were in early to moderate stages of the disease according to the Hoehn and Yahr scale [Goetz et al., 2004]. The severity of their motor symptoms was evaluated during the ON state, using the motor examination score of the Unified Parkinson's Disease Rating Scale part III (motor UPDRS) Goetz et al., 2008]. Fourteen patients had presented with right body side onset of motor symptoms while 10 patients had exhibited left side onset of motor symptoms. All patients were treated with dopaminergic therapy, including various combinations of levodopa, dopamine agonists, amantadine, and monoamine oxidase B (MAO-B) inhibitors. The levodopa equivalent daily dose (LEDD) was calculated according to [Tomlinson et al., 2010].

## Controls

Thirty-four age-matched healthy subjects, without prior history of neurological or psychiatric disorders participated in the study.

The patient and control groups were well matched with respect to gender ($P = 0.84$, Fisher exact test) and age ($P = 0.96$, two sample $t$-test).

## MR Imaging

Image acquisition was carried out on a 3T whole-body system (Trio TIM, Siemens AG, Erlangen, Germany) using a standard 12-channel head coil. Foam padding was used to stabilize the subject head. The subjects were asked to remain still with eyes open for the duration of the scanning session. The patients were studied under medication, in ON state, to minimize the effects of head motion.

$T_1$-weighted anatomical images were acquired with a MPRAGE sequence, with the following imaging parameters: resolution = 1 mm isotropic, field of view (FOV) = 192 × 256 × 160 $mm^3$, matrix = 192 × 256 × 160, repetition time (TR)/echo time (TE)/inversion time (TI) = 1,620/3.87/950 ms, flip angle = 15°.

Resting state whole brain perfusion data were acquired using an optimized ASL sequence [Vidorreta et al., 2013], with the following parameters: pseudo-continuous labeling (Hanning-shaped RF pulses, peak $B_1 = 53$ mG, RF duration = 500 μs; $G_{average} = 0.6$ G/cm, labeling duration = 1,600 ms, post-labeling delay = 1,530 ms), followed by a background suppressed 3D GRASE readout (TR = 3.5 s, TE = 55.7 ms, resolution = 4 × 4 × 7 $mm^3$, FOV = 250 × 188 × 112 $mm^3$, 16 nominal partitions with 12.5% oversampling, 5/8 partial Fourier, matrix size = 64 × 49 × 11, bandwidth (BW) = 2,790 Hz/pixel, gradient echo (GE) spacing = 0.4 ms (with ramp sampling), spin echo (SE) spacing = 26 ms, read-out time = 270 ms). Two nonselective inversion pulses (15.35 ms duration and 220 mG amplitude) were added for background suppression (BS) with inversion times $TI_1 = 1{,}800$ ms; $TI_2 = 500$ ms. Bipolar gradients ($b = 5$ s/$mm^2$) were used to suppress intravascular signal. The spatial extent of the inversion plane was 1 cm and it was offset 8 cm from the center of the imaging slab so that it was located at the base of the cerebellum. The coverage of the imaging slab included the cerebrum and superior part of the cerebellum. A scan time of 6 min was used to acquire 50 pairs of label and control images, followed by a short scan of five pairs acquired without BS, that were required for calculation of cerebral blood flow (CBF). Raw perfusion data were saved and reconstructed off-line.

## Data Preprocessing

Data preprocessing and analyses were carried out using custom scripts in Matlab (Mathworks, MA) and SPM (version 8, Wellcome Trust Center for Neuroimaging, University College London, UK).

Label and control images were realigned, coregistered to the anatomical dataset and pairwise subtracted to obtain the perfusion imaging time series. Those images identified as outliers (i.e., when the global perfusion signal differed from the mean of the perfusion signal time series by ±2 standard deviations) were replaced by the average of the two adjacent images [Wang et al., 2008]. Individual perfusion images were masked to remove out-of-brain voxels and CBF images were computed, using the single compartment ASL perfusion model, as previously described [Wang et al., 2005].

The $T_1$-weighted anatomical images were normalized to a study-specific gray matter template, generated using the Diffeomorphic Anatomical Registration through Exponentiated Lie algebra algorithm [Ashburner, 2007]. The individual CBF maps were then normalized to the same template, mapped into MNI space using an affine transformation, resliced to an isotropic voxel size of 1.5 mm and spatially smoothed using a 6 mm full-width at half-maximum Gaussian kernel.

## Analysis of Head Movement Parameters

The translational ($x$, $y$, $z$) and rotational ($\alpha$, $\beta$, $\gamma$) movement parameters obtained during the realignment step were analyzed to assess differences in the amount of movement between patients and controls. For each subject, the average root mean square (RMS) values of the six movement parameters were calculated. Differences in movement between groups were evaluated using a multivariate analysis of variance (MANOVA), with the movement parameters RMS values as the dependent variables.

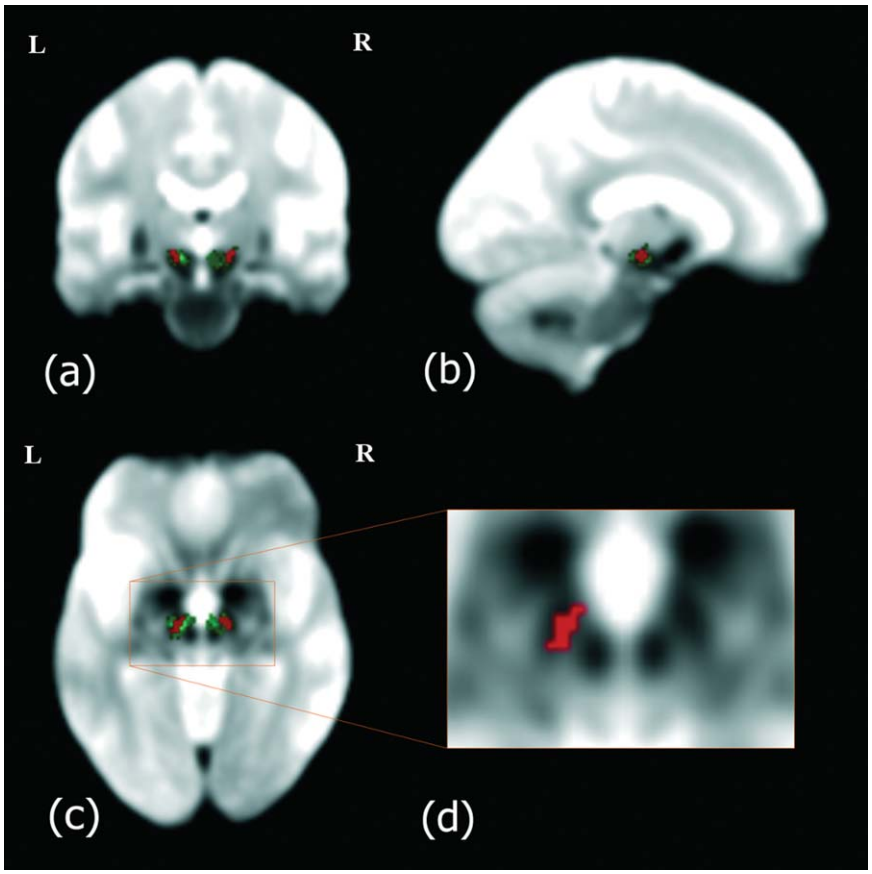


**Figure 1.**

T2*-weighted group mean image: (**a**) coronal, (**b**) sagittal, and (**c**) axial orientations. The STN can be visualized as a hypointense area located ventro-lateral to the rostral portion of the red nucleus [see the magnified view in (**d**)]. The STN atlas (in green) and the STN mask used as seed (in red) have been overlaid on the anatomical image. The STN mask was delineated manually to include hypointense areas comprised within the probabilistic STN atlas. The images are displayed in neurological orientation.

## Localization of the STN

The STN can be identified in $T_2$*-weighted images as a low signal intensity area with a dorsolateral to ventromedial orientation [Andrade-Souza et al., 2008; Massey and Yousry, 2010]. $T_2$*-weighted images of the study subjects acquired during other fMRI experiments were used for STN localization, following the procedure described by Baudrexel et al. [2011]. The $T_2$*-weighted imaging series had been acquired using a standard gradient echo echo-planar imaging sequence, with the following parameters: TR = 3 s, TE = 30 ms, isotropic resolution = 3 mm, FOV = 192 × 192 $mm^2$, 49 slices, matrix size = 64 × 64, BW = 2,790 Hz/pixel and number of volumes = 300. Each individual $T_2$*-weighted imaging series was averaged and normalized to the study-specific template. The normalized individual mean images were then averaged to obtained a $T_2$*-weighted group mean image. The right and left STN masks were manually delineated based on this image (Fig. 1), using the FSL 4.1.9 viewer (http://fsl.fmrib.ox.ac.uk/fsl/fslwiki/) and an atlas probability map of the STN, available in electronic format [Forstmann et al., 2012]. The mask included only hypointense voxels located dorsolateral to the SN in the coronal view that belonged to the STN according to the probability map.

The resulting STN ROIs had the following features: right STN: center of mass [12.1, −12.7, −6.77]; volume = 152 $mm^3$; min/max $x$ [9, 15], $y$ [−15, −10], $z$ [−9, −4]; left STN: center of mass [−11, −13.4, −6.92]; volume = 149 $mm^3$; min/max $x$ [−15, −7], $y$ [−17, −10], $z$ [−9, −4].

## FC analysis

The FC analysis was carried out using the FC toolbox [Whitfield-Gabrieli and Nieto-Castanon, 2012], to evaluate the temporal correlations in the slow spontaneous fluctuations in the resting state CBF time series. A seed-based

approach was used, by selecting as seeds the two ROIs located in the right and left STN, respectively.

Two preprocessing steps were carried out before the Pearson's correlation analysis. First, several covariates were removed from the data by linear regression, to eliminate spatial correlations due to physiological noise. The covariates included the movement parameters and the average signals extracted from six ROIs, two located within the white matter and four in the ventricles [as in Viviani et al., 2011]. The CBF signal in the ventricles and in areas surrounding major blood vessels is affected by vascular pulsation. Dagli et al. [1999] demonstrated that cardiac induced signal variance is localized to these specific areas. Removing the averaged CBF signal in the ventricular ROIs was expected to remove cardiac induced signal fluctuations. The average CBF signal in the white matter ROIs is known to be affected by the respiratory cycle [Windischberger et al., 2002]. Removing the averaged CBF signal in the white matter ROI was expected to reduce respiration-related signal fluctuations.

The signal in the CBF time series was then filtered using a low-pass filter ($f < 0.07$ Hz). No high pass filter was used since the CBF time series does not suffer from the low frequency drift present in the BOLD data.

Voxelwise seed-to-voxel connectivity was estimated using Pearson's correlation, followed by Fisher's $r$-to-$z$ transformation. Two individual $z$-maps representing the strength of correlation of each brain voxel with each of the seeds were obtained. These maps were entered into the second level random effect analyses.

First, right and left STN z-maps of the control subjects were evaluated using one-sample $t$-tests to obtain group connectivity maps of the healthy STN. These connectivity maps were thresholded using a voxel level $P$-value of 0.05 (FWE-corrected). In this case, a voxel-level threshold was preferred over a cluster-extent threshold to avoid the low spatial specificity introduced by cluster-extent-based thresholding in the presence of large clusters [Woo et al., 2014].

Next, right and left STN $z$-maps obtained from all subjects were entered into a $2 \times 2$ ANOVA, set up using a flexible factorial design with two factors: group (controls, patients) and STN side (right, left). The model included the main effects of group and STN side and the interaction between these two factors. The results of this analysis revealed a significant effect of group. No significant interaction between group and STN side was found. A post-hoc comparison between the two levels of the factor group was then realized to evaluate between-group differences. These differences were assessed at a cluster-level $P$-value of 0.05 (FWE-corrected), after thresholding the$T$-maps with a cluster defining threshold of $P < 0.001$.

Cluster volume and local maxima labeling was performed using SPM Anatomy toolbox [Eickhoff et al., 2005] and the Talairach Daemon [Lancaster et al., 2000]. For the identification of cortical gyri, Petrides's atlas on the human cerebral cortex was used [Petrides, 2012].

### Extraction of FC Values from ROIs

The comparison of STN connectivity maps between patients and controls yielded two significant clusters (see Results section for details). The maxima of these clusters were located at the left precentral gyrus (MNI coordinates = [−34, −14, 58]) and at the right precuneus (MNI coordinates = [8, −62, 48]), respectively. Spherical ROIs of 3 mm radius were defined at these locations. Individual $z$-values in these ROIs, representing the strength of the correlation between the STN time series signal and the signal at these locations, were extracted from the right and left STN connectivity maps in the patient group.

### Correlations of Connectivity Strength with Clinical Variables

Shapiro–Wilks normality tests were carried out to ensure that the extracted $z$-values were normally distributed. The pairs of extracted $z$-values from each ROI were entered into separate multivariate general linear models (GLM), with independent variables: UPDRS ON, Hoehn and Yahr stage, disease duration and LEDD. The GLMs were implemented using the MANOVA function in the R software package. Statistical significance was assessed at $P < 0.05$, after Bonferroni correction for multiple comparisons.

### Discriminatory Performance of the FC Indexes

ROC analysis and binary logistic regression were used to assess how well the extracted FC $z$-values from the ROIs listed above were able to discriminate between PD patients and controls. The discriminatory performance of the four indexes was evaluated separately. Additionally, the four indexes were combined using a binary logistic regression model and the performance of this model was also assessed. In each case, the area under the ROC curve (AUC) and 95% confidence intervals (CI) were calculated using nonparametric methods [Robin et al., 2011]. Leave-one-out cross-validation was used to assess the validity of the results.

### Additional FC Analyses

Due to the small volume of the STN, relative to the voxel size of the CBF images, the signal extracted from the STN could suffer from partial voluming of other adjacent structures into the STN mask. To evaluate the anatomical specificity of the results, three additional FC analyses were carried out, with seeds in the SN and in two thalamic nuclei: the ventral lateral posterior nucleus (ventral part, VLpv) and the ventral lateral anterior nucleus (VLa), which are the two thalamic nuclei located closer to the STN. The SN masks were obtained from a probability atlas map, available in electronic format [Keuken et al., 2014].

The VLa and VLpv masks were obtained from a 3D atlas of the human thalamus, also available in electronic format [Krauth et al., 2010]. Details of these analyses and their results are presented in Supporting Information.

## RESULTS

### Head Movement Parameters

Mean and standard deviation of the movement parameters RMS values, measured in the control group were: $x = 0.12 \pm 0.11$ mm, $y = 0.13 \pm 0.08$ mm, $z = 0.31 \pm 0.30$ mm, $\alpha = 0.34 \pm 0.42$ degrees, $\beta = 0.15 \pm 0.14$ degrees, $\gamma = 0.14 \pm 0.09$ degrees, and in the patient group: $x = 0.15 \pm 0.15$ mm, $y = 0.17 \pm 0.12$ mm, $z = 0.31 \pm 0.22$ mm, $\alpha = 0.41 \pm 0.36$ degrees, $\beta = 0.17 \pm 0.17$ degrees, $\gamma = 0.23 \pm 0.19$ degrees.

According to the MANOVA results, there were no significant differences in the amount of movement between groups ($P = 0.061$).

### FC of the STN in Healthy Controls

Connectivity maps in healthy controls were thresholded at a voxel-level $P$-FWE of 0.05 ($T > 5.89$), and a cluster size extent $k > 15$ (Table II and Fig. 2). At this significance threshold, both left and right STN showed the strongest correlations within the seed voxels as expected, as well as bilateral positive correlations with the thalamus, medial and lateral globus pallidus, and ventral midbrain. In addition, areas of positive correlation were also observed in the putamen, amygdaloid complex, hippocampal complex, parahippocampal gyrus, fusiform gyrus, inferior temporal gyrus, and insular cortex. No areas of negative correlation were observed.

### Parkinson's Disease-Related Alterations in FC

The comparison of STN connectivity maps between patients and controls only showed areas of increased connectivity in PD patients with respect to the controls (Table III and Fig. 3). No areas of decreased connectivity were found.

FC of the STN was increased in the PD patients in two clusters. One cluster was located dorsally in the left precentral gyrus extending into the postcentral gyrus, primarily occupying primary motor, premotor, and somatosensory cortices. The second cluster was located bilaterally in the precuneus, but was larger in the right hemisphere extending into the paracentral lobule anteriorly and the superior parietal lobule, laterally. No changes were found in any subcortical structure.

### Correlations of Connectivity Strength with Clinical Variables

As described above, the comparison of STN connectivity maps between patients and controls yielded two significant clusters of increased connectivity in the patients, with maxima in the left precentral gyrus ([−34, −14, 58]) and right precuneus ([8, −62, 38]), respectively. The results of the multivariate GLM for ROI 1 (left precentral gyrus) showed a significant effect of LEDD (Pillai trace = 0.4127, $F$ (2,18) = 6.3244, $P = 0.0083$) on the connectivity strength within the patient group (Fig. 4). For ROI 2 (right precuneus), no significant effects were found.

### Discriminatory Performance of the FC Indexes

The results of the ROC analysis indicated that the combination of the four connectivity indexes using a binary logistic regression model (Supporting Information Table I for details of the model), had the highest power to discriminate PD subjects from controls, with an AUC of 0.89 (95% CI = 0.79–0.96; Table IV). At a cutoff of 0.40, where the sensitivity and specificity curves intersected, the sensitivity, specificity, and classification accuracy were 83.3, 79.4, and 81%, respectively. Leave-one-out cross validation showed a cross-validated AUC of 0.82 (95% CI = 0.75–0.94).

### Additional FC Analyses

The results of the FC analysis carried out placing seeds in the SN showed no significant differences in connectivity between patients and controls. The FC analyses with seeds in two thalamic nuclei (VLpv and VLa) revealed increased connectivity in the patients in specific cortical areas (for details, see Supporting Information). However, these areas were different from the areas that exhibited hyperconnectivity with the STN. Therefore, these results support the specificity of the findings of increased connectivity between the STN and the left precentral gyrus and right precuneus, described above.

## DISCUSSION

In this study the resting state FC of the STN was investigated both in healthy controls and PD patients, using ASL perfusion-based fcMRI techniques.

### FC of the STN in Healthy Controls

The FC analysis based on the temporal correlations in the CBF signal in controls revealed in the first place strong connections with the ventral midbrain, pallidal complex, and thalamus. These findings are consistent with those reported in two previous BOLD fcMRI studies [Baudrexel et al., 2011; Brunenberg et al., 2012].

The STN projects heavily to the substantia nigra reticulata (SNr) and internal globus pallidus (GPi), and is reciprocally connected to the external globus pallidus (GPe). More recent anatomical studies have also identified bilateral reciprocal connections of the STN with the caudal

**TABLE II. Functional connectivity of the STN in healthy controls (voxel *P*-FWE < 0.05; *T* > 5.89; *k* > 15)**

| | | Local maxima | | |
|---|---|---|---|---|
| Cluster size | Cluster distribution | Anatomical region | MNI coordinates [x, y, z] | *T* |
| Left STN | | | | |
| 2,891 | 7.4% (32.3%) L Thalamus–prefrontal | L Subthalamic nucleus | −10, −12, −8 | **42.49** |
| | 5.0% (16.6%) R Hippocampus (CA) | R Hippocampus (HATA) | 18, −10, −10 | 10.84 |
| | 4.6% (24.2%) R Hippocampus (SUB) | R Substantia nigra | 12, −14, −12 | 10.46 |
| | 3.7% (18.1%) R Thalamus–prefrontal | R Fusiform gyrus | 32, −30, −26 | 9.28 |
| | 3.3% (11.6%) L Hippocampus (CA) | L Fusiform gyrus | −28, −32, −22 | 7.63 |
| | 2.6% (13.8%) L Hippocampus (SUB) | R Amygdala (CM) | 26, −6, −6 | 7.62 |
| | 1.5% (34.0%) L Thalamus–premotor | R Globus pallidus | 28, −10, −2 | 7.59 |
| | 1.4 % (21.6%) R Amygdala (SF) | L Globus pallidus | −20, 0, 2 | 7.37 |
| | 1.3% (65.8%) L Amygdala (CM) | | | |
| | 1.2 % (16.4%) L Amygdala (SF) | | | |
| | 1.1% (5.4%) L Thalamus–temporal | | | |
| | 1.0 % (39.6%) R Amygdala (CM) | | | |
| | 65.9% Not assigned or less than 1% | | | |
| 247 | 8.7% (8.4%) R Parietal operculum (OP 3) | R Insula lobe | 44, 12, −2 | 9.19 |
| | 2.9% (1.4 %) R Parietal operculum (OP 4) | R Rolandic operculum | 46, −6, 8 | 7.03 |
| | 88.4% Not assigned or less than 1% | R Insula lobe | 44, 2, 6 | 6.94 |
| 60 | 72.1% (13.0%) R Amygdala (LB) | R Hippocampus | 34, −4, −22 | 8.14 |
| | 2.9% (0.2%) R Hippocampus (CA) | R Amygdala (LB) | 28, 0, −22 | 6.27 |
| | 1.5% (0.4%) R Human Intraparietal Area (hIP1) | | | |
| | 23.5% Not assigned or less than 1% | | | |
| 25 | 100% Not assigned or less than 1% | R Medial temporal pole | 38, 4, −36 | 6.75 |
| 17 | 89.0% (3.0%) R Parietal operculum (OP 1) | R Rolandic operculum | 46, −28, 22 | 6.57 |
| | 11.0% (0.7%) R Inferior parietal cortex (PFop) | | | |
| | 0% Not assigned or less than 1% | | | |
| 17 | 5.9% (0.1%) R Cerebellum lobule V | R Lingual gyrus | 16, −42, −12 | 6.49 |
| | 94.1% Not assigned or less than 1% | | | |
| Right STN | | | | |
| 1,904 | 15.1% (48.2%) R Thalamus–Prefrontal | R Subthalamic nucleus | 12, −14, −8 | **41.61** |
| | 11.1% (31.5%) L Thalamus–prefrontal | L Thalamus–prefrontal | −10, −12, 0 | 11.47 |
| | 3.7% (48.0%) R Thalamus–premotor | R Fusiform gyrus | 30, −34, −24 | 7.59 |
| | 2.1% (7.3%) R Hippocampus (SUB) | R Thalamus–Prefrontal | 6, −26, 0 | 7.29 |
| | 2.0% (4.3%) R Hippocampus (CA) | R Parahippocampal gyrus | 30, −16, −30 | 7.04 |
| | 1.8% (5.6%) R Thalamus–Temporal | L Thalamus–parietal | −20, −24, 8 | 6.94 |
| | 1.8% (25.9%) L Thalamus–Premotor | | | 6.68 |
| | 1.7 % (36.4%) R Thalamus–Somatosensory | | | 6.11 |
| | 1.6% (8.7 %) R Thalamus–parietal | | | 5.96 |
| | 1.0 % (3.1%) L Thalamus–temporal | | | |
| | 58.1% Not assigned or less than 1% | | | |
| 86 | 58.7% (16.3%) L Amygdala (LB) | L Amygdala (LB) | −24, 0, −24 | 8.03 |
| | 21.1% (9.2 %) L Hippocampus (EC) | | | |
| | 2.3% (2.1%) L Amygdala (SF) | | | |
| | 17.9% Not assigned or less than 1% | | | |
| 55 | 100% Not assigned or less than 1% | R Insula lobe | 46, 10, −2 | 6.79 |
| | | R Insula lobe | 40, 12, −8 | 6.48 |
| | | R Insula lobe | 32, 16, −10 | 6.33 |
| 42 | 100% Not assigned or less than 1% | L Insula lobe | −40, 8, −4 | 6.53 |
| 31 | 6.9%(0.6%) R Amygdala (LB) | Middle temporal gyrus | 42, 0, −28 | 7.55 |
| | 83.1% Not assigned or less than 1% | | | |
| 23 | 2.2%(0.1%) R Hippocampus (CA) | R Fusiform gyrus | 36, −44, −12 | 6.23 |
| | 87.8% Not assigned or less than 1% | | | |
| 18 | 10.5%(1.6%) R Insula | R Putamen | 34, −20, −4 | 7.01 |
| | 89.5% Not assigned or less than 1% | | | |

Local maxima are shown in MNI coordinates (in mm). BA: Brodmann area. R: right. L:left. Cluster distribution was assessed with the Anatomy toolbox. The cluster distribution is given as **a**% (**b**%), where **a** is the percentage of the cluster that lies in a specific area and **b** is the percentage of this area occupied by the cluster.

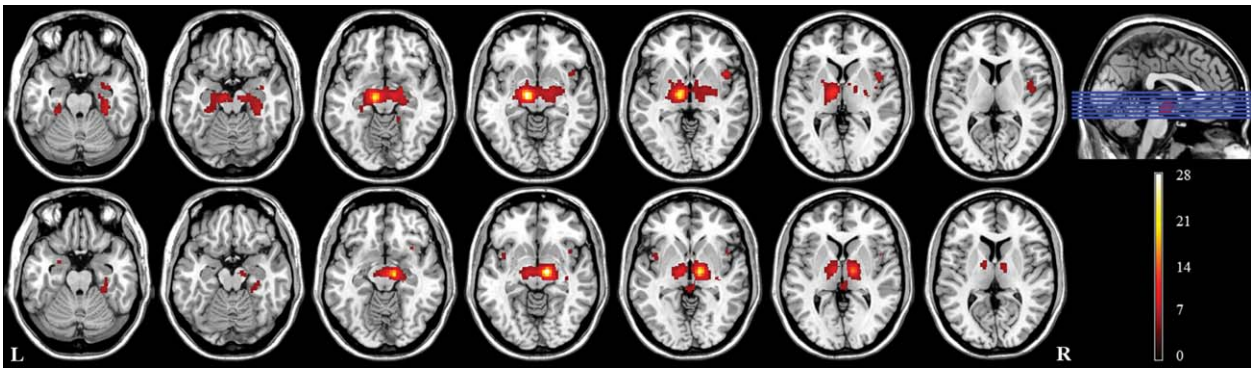


**Figure 2.**

Areas functionally connected with the left (top row) and right (bottom row) STN in healthy controls ($P < 0.05$, FWE corrected at the voxel level, $T > 5.89$, $k > 15$), overlaid on anatomical axial $T_1$-weighted images, displayed in neurological orientation. The location of the axial slices in the inferior-superior direction is indicated by the blue lines in the sagittal view. The color scale represents the value of the *T*-statistic.

intralaminar thalamic nuclei, as well as less prominent subthalamothalamic projections to the ventral anterior–ventral lateral complex [Castle et al., 2005; Rico et al., 2010]. Thus, the results presented here show that the STN, in addition to being anatomically connected with these subcortical structures, is also functionally connected with them in the resting state.

At the cortical level, both STN were functionally connected with the right insular cortex and bilaterally with the hippocampal complex, parahippocampal and fusiform gyri, and the amygdala. The insular cortex projects to the STN in rat and primate [Canteras et al., 1990; Kelly and Strick, 2004], whereas the hippocampal complex receives projections from an area adjacent to STN in the posterior lateral hypothalamus [Kelly and Strick, 2004], which has been denominated parasubthalamic nucleus (para-STN), as many of the afferents to the STN extend medially into this area [Goto and Swanson, 2004; Haynes and Haber, 2013]. Finally, the amygdala also projects to the STN and has reciprocal connections with the para-STN [Kelly and Strick, 2004]. Anatomical studies using MRI diffusion tractography in the human brain have also reported strong connectivity of the STN with all the aforementioned structures, and specifically two distinct clusters in the hippocampus and insular cortex bilaterally were particularly robust in the majority of subjects [Lambert et al., 2012].

The resting state FC of the STN with the parahippocampal and fusiform gyri was also observed in one of the previous BOLD studies [Brunenberg et al., 2012]. While there are evidences that the basal ganglia and the hippocampal complex interact to accomplish specific learning behaviors [DeCoteau et al., 2007; Fernandez-Seara et al., 2009; Miyoshi et al., 2012], the present results suggest that the STN and the hippocampus are also functionally connected in the resting state.

Resting state FC of the STN with the insular cortex was not observed in any of the two previous BOLD fcMRI studies, although other medial and lateral frontal areas were reported [Brunenberg et al., 2012]. However, FC of the caudate nucleus and putamen with the insular cortex has been reported in healthy subjects and PD patients [Helmich et al., 2010; Postuma and Dagher, 2006]. A study using diffusion-weighted imaging tractography and functional MRI has demonstrated that the inferior frontal cortex and the adjacent insular cortex are connected to the STN via a white matter tract, and that these two structures are part of an executive control network that plays a key role in motor response inhibition [Aron et al., 2007; Aron and Poldrack, 2006].

## Parkinson's Disease-Related Alterations in STN FC

The STN in PD patients showed increased FC with two cortical areas in comparison with the controls. One of the hyperconnected clusters was located in the left primary and secondary motor cortices. This finding is consistent with those reported by Baudrexel et al. [2011] who also observed increased FC of both STN primarily with the left motor cortex.

The STN receives direct cortical projections from the frontal lobe, constituting what has been regarded as the hyperdirect cortico-STN pathway within the model of basal ganglia function [Haynes and Haber, 2013; Nambu et al., 2002]. Recent research has highlighted the role of pathological electrophysiological oscillatory activity in the Parkinsonian state, particularly in the beta frequency band [DeLong and Wichmann, 2007]. Specifically, pathological coherent activity between the STN and primary motor cortex has been suggested to underlie PD circuit dysfunction

**TABLE III. Areas of increased functional connectivity with the STN in the PD patients with respect to the controls (cluster-corrected *P*-value < 0.05, cluster defining threshold *P* < 0.001)**

| Cluster size Cluster corrected *P* | Cluster distribution | Local maxima | | |
|---|---|---|---|---|
| | | Anatomical region | MNI coordinates [*x*, *y*, *z*] | T |
| 667 | 41.7% (6.3%) L BA 6 | L Precentral gyrus (BA 6) | −34, −14, 58 | **5.13** |
| <0.0001 | 19.2% (10.5%) L BA 4a | L Precentral gyrus (BA 4p) | −24, −26, 54 | 4.42 |
| | 15.0% (17.7%) L BA 4p | L Precentral gyrus (BA 4p) | −30, −14, 46 | 3.98 |
| | 6.4% (8.1%) L BA 3a | L Precentral gyrus (BA 4p) | −16, −30, 54 | 3.87 |
| | 1.0% (0.8%) L BA 2 | L Precentral gyrus (BA 4a) | −14, −28, 58 | 3.84 |
| | 16.7% Not assigned or less than 1% | L Postcentral gyrus (BA 3b) | −28, −36, 52 | 3.36 |
| 920 | 11.1% (8.6%) R SPL (7A) | R Precuneus (SPL 7A) | 8, −62, 48 | 4.83 |
| <0.0001 | 10.3% (21.6%) R SPL (5M) | L Precuneus | −10, −50, 52 | 4.74 |
| | 9.1% (13.0%) R SPL (5L) | R Precuneus (SPL 5M) | 14, −48, 52 | 4.68 |
| | 6.7% (6.4%) R BA 2 | R Precuneus (SPL 5L) | 8, −52, 60 | 4.25 |
| | 6.1% (15.4%) L SPL (5M) | R Superior parietal Lobule (SPL 7A) | 18, −56, 58 | 4.25 |
| | 5.9% (5.9%) R BA 3b | R Superior parietal Lobule (SPL 7PC) | 16, −54, 54 | 4.19 |
| | 3.9% (7.2%) R BA 3a | R Paracentral lobule (BA 3b) | 16, −40, 58 | 4.08 |
| | 2.4% (1.2%) L SPL (7A) | R Precuneus (SPL 7P) | 10, −72, 50 | 3.79 |
| | 2.2% (3.0%) R SPL (7P) | R Postcentral gyrus (BA 3b) | 22, −34, 64 | 3.62 |
| | 2.0% (3.9%) R BA 4p | L Precuneus | −2, −54, 46 | 3.60 |
| | 1.2% (0.9%) R BA 4a | | | |
| | 1.2% (6.3%) R SPL (7M) | | | |
| | 1% (2.3%) R SPL (7PC) | | | |
| | 36.9% Not assigned or less than 1% | | | |

Local maxima are shown in MNI coordinates (in mm). Cluster distribution was assessed with the Anatomy toolbox. The cluster distribution is given as **a**% (**b**%), where **a** is the percentage of the cluster that lies in a specific area and **b** is the percentage of this area occupied by the cluster. BA: Brodmann area. R: right. L: left. SPL: Superior Parietal Lobule.

[Marreiros et al., 2013; Moran et al., 2011; Shimamoto et al., 2013], while restoration of normal cortical firing rates ameliorated parkinsonian symptoms in rats [Degos et al., 2009; Gradinaru et al., 2009]. The enhanced FC between STN and cortical motor areas is consistent with the abnormal beta band coherence observed between them at rest [Hirschmann et al., 2011; Litvak et al., 2011], although a direct relationship between the slow fluctuations detected by fMRI and the beta band oscillatory activity has not yet been demonstrated. Nonetheless, a relationship has been found between the BOLD fluctuations and power modulations of the local field potential (LFP). Although the gamma band is the frequency band that holds the strongest relationship (i.e., the amplitude of the BOLD signal scales with gamma power), the LFP power in other frequency bands, specially the beta band, is also related to the BOLD signal [Magri et al., 2012; Pan et al., 2013]. In addition, connectivity studies assessing the spatial correlation between resting state networks identified using BOLD and magnetoencephalography (MEG) data have shown that the best match occurs when MEG connectivity is assessed via correlations in the beta frequency band [Hall et al., 2014].

The cluster of increased connectivity in the motor cortex was located in the left hemisphere (a smaller cluster found in the right hemisphere did not survive the cluster level correction for multiple comparisons), similarly to the previous BOLD study [Baudrexel et al., 2011]. A possible explanation for this could be related to handedness, as in both studies all subjects were right-handed and thus, likely left-hemisphere dominant.

The strength of the connectivity values in this cluster was found to correlate with the levodopa dose in the patient group. Litvak et al. [2011] also reported an increase of cortico-subthalamic beta coherence with dopaminergic medication in prefrontal regions, in PD patients. Kelly et al. [2009] observed a levodopa-induced increase in FC in motor networks, in healthy volunteers. Stoffers et al. [2008a] reported elevated levels of cortico-cortico FC in PD patients versus controls, measured using magnetoencephalography, and further increases in ON versus OFF states [Stoffers et al., 2008b]. These studies suggest that FC within frontostriatal circuits is subject to modulation by dopaminergic therapy.

The second cortical area of increased FC with the STN in PD patients, was located bilaterally in the medial posterior parietal cortex or precuneus, although in the right hemisphere it extended both laterally and anteriorly, occupying not only Brodmann's area 7, but also areas 5 and 3b (Table III). The precuneus is a complex area that plays a core role not only in the default-mode network but also more broadly in cognition through its engagement with

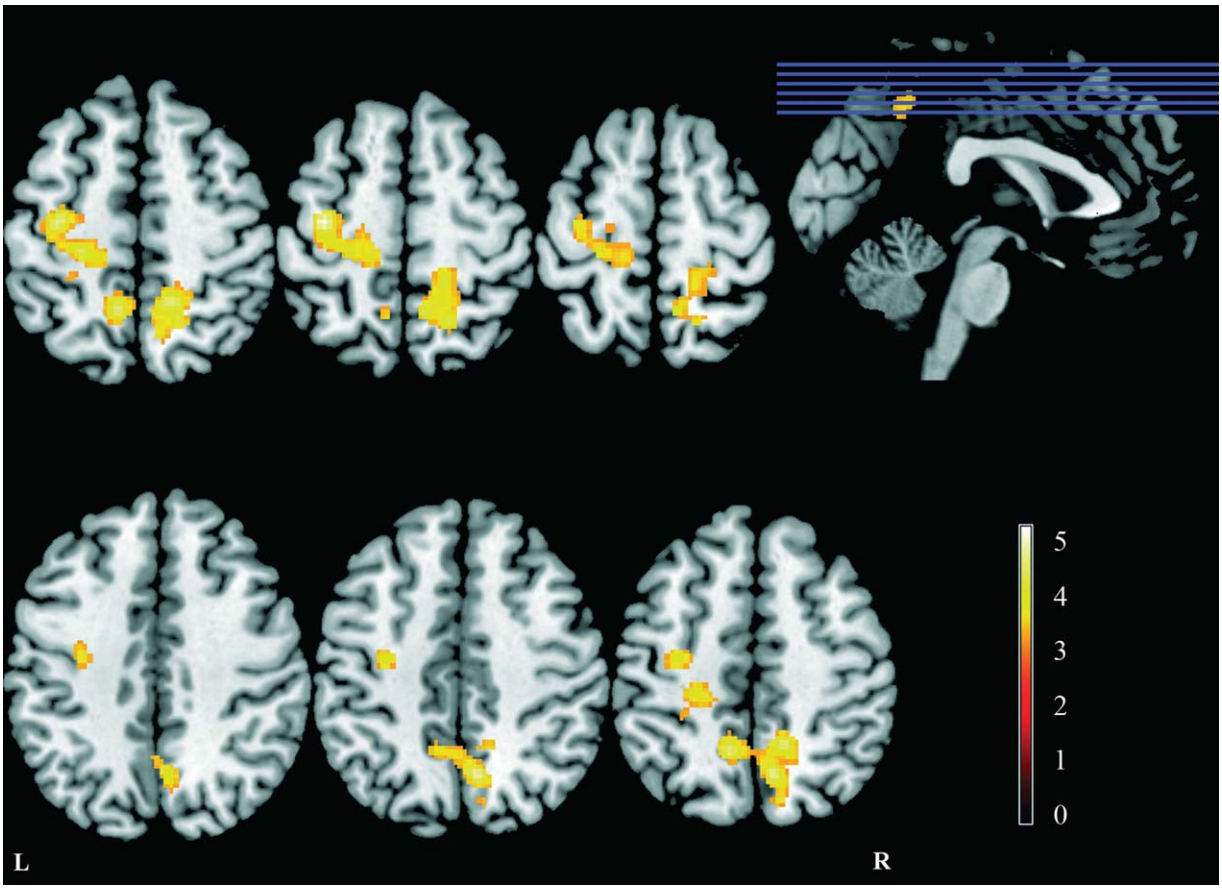


**Figure 3.**

Areas of increased FC with the STN in patients with respect to controls ($P < 0.05$, FWE corrected at the cluster level), overlaid on anatomical axial $T_1$-weighted images, displayed in neurological orientation. The location of the axial slices in the inferior-superior direction is indicated by the blue lines in the sagittal view. The color scale represents the value of the *T*-statistic.

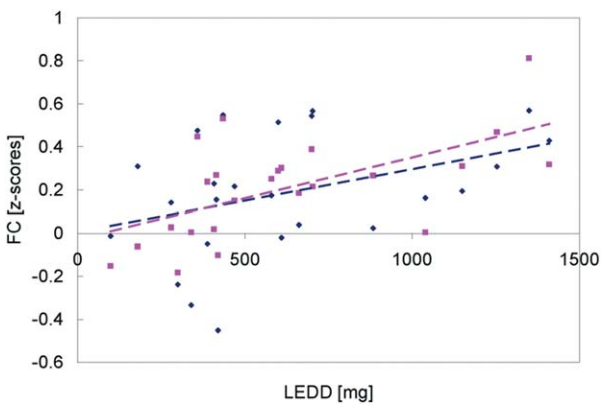


**Figure 4.**

Correlation between the FC strength of the STN with the left motor cortex (*y*-axis) and the levodopa dose (*x*-axis), across the patient group. Right STN values are shown in pink, while left STN values are shown in blue.

different neural networks under a variety of processing states [Cavanna and Trimble, 2006].

Although no direct connections between STN and the parietal cortex have been reported, the SNr, one of the

**TABLE IV. Results of ROC analysis for the discrimination between PD patients and controls**

| Functional connectivity index | AUC (95% CI) |
|---|---|
| Right STN–left precentral gyrus | 0.83 (0.73–0.94) |
| Left STN–left precentral gyrus | 0.75 (0.61–0.89) |
| Right STN–right precuneus | 0.75 (0.62–0.88) |
| Left STN–right precuneus | 0.79 (0.66–0.92) |
| Combination of the four indexes | 0.89 (0.80–0.98) |

Column 1 describes the FC index used as classifier and column 2 gives the area under the ROC curve (AUC) and the 95% confidence intervals (CI).

main target nuclei of STN, projects via the thalamus to a subregion of area 7b in the primate [Clower et al., 2005].

This indirect anatomical pathway represents the first evidence of a link between the basal ganglia output and the parietal cortex [Clower et al., 2005] providing an anatomical route to explain some of the nonmotor deficits observed in PD patients involving aspects of visuomotor and visuospatial integration, which are generally ascribed to dysfunction of the posterior parietal cortex [Pereira et al., 2009]. The precuneus–STN FC abnormalities found in this work could underlie some of these cognitive deficits. Future studies should be carried out to confirm these abnormalities, because they can provide additional evidence to that from other imaging techniques reporting precuneus alterations in PD like cortical thinning [Jubault et al., 2011; Pagonabarraga et al., 2013], hypometabolism [Tang et al., 2010], and hypoperfusion [Fernandez-Seara et al., 2012], further suggesting that this area is specifically affected in PD.

### Discriminatory Performance of the FC Indexes

The strength of the functional connections STN-motor cortex and STN-precuneus provided good discrimination between PD patients and controls. Only a previous study has attempted to use FC metrics combined with structural MRI measures as a classification tool in PD [Long et al., 2012]. The classification results presented here are preliminary, since they have not been verified in a separate group. Nonetheless, they suggest that STN FC metrics derived from ASL data, could have diagnostic power in early PD and warrant further investigation.

### Methodological and Technical Considerations

In this study, PD patients were assessed under their current medication in ON state, in order to minimize the effects of head motion. Baudrexel et al. [2011] studied patients in OFF state, with similar findings. The fact that STN FC increases have been observed in PD patients in ON state suggests that these FC increases are not primarily due to resting tremor, which is attenuated by dopaminergic therapy [Fishman, 2008]. In addition, connectivity increases have not been observed in the thalamus, which is one of the key regions involved in tremor [Helmich et al., 2012]. In their study, Baudrexel et al. [2011] found similar increases in FC between the STN and motor cortex both in patients with tremor and in patients with akinetic-rigid PD type. Helmich et al. [2010] found changes in connectivity in PD that were similar in tremor dominant and nontremor patients. Taken together these observations suggest that resting tremor is not the main cause of connectivity abnormalities in PD, although the presence of tremor-related signal fluctuations cannot be ruled out.

The results presented here have been obtained using a seed-based correlation analysis. The seed location was determined based on an atlas probability map of the STN and T2*-weighted MR images of the study subjects, where the STN was visualized as a hypointense area. This localization method is preferable to extracting the seed ROIs from a brain atlas only, because it takes into account the individual brain anatomy, which is especially important when studying elderly subjects. Only voxels that appeared clearly hypointense were included in the STN ROIs. In the $z$ direction, only voxels with $z$ coordinates above $-9$ mm were selected to avoid the SN. Thus, the size of the STN ROIs was comparable to previous estimations of the human STN volume [Levesque and Parent, 2005; Yelnik, 2002]. This procedure was expected to guarantee that the perfusion signal was extracted reliably from the STN, avoiding adjacent anatomical structures, to ensure the anatomical specificity of the results. In addition, the results of FC analyses carried out with seeds in the SN and in the VLpv and VLa thalamic nuclei support the specificity of the STN results.

### ASL Perfusion-Based fMRI for the Assessment of Resting State FC

Assessment of the brain FC in the resting state is generally carried out by evaluating temporal correlations in the fMRI signal acquired using a T2*-weighted sequence, sensitive to BOLD contrast. However, early on Biswal et al. [1997] demonstrated that FC maps of the sensorimotor network could also be obtained using ASL perfusion-based fMRI, albeit with lower sensitivity. Technical improvements in ASL in recent years have dramatically increased the SNR of the technique [Fernandez-Seara et al., 2008] and enhanced its power for task activation detection [Vidorreta et al., 2013]. A similar improvement in statistical power was expected in studies of resting state FC. The results of this study show that ASL fcMRI has enough sensitivity to assess FC changes in neurodegenerative diseases.

## CONCLUSIONS

The results presented here provide evidence of abnormal STN-cortical FC in specific brain areas of PD patients, involved in motor and nonmotor processes. The strength of the abnormal FC values showed discriminatory power between patients and healthy controls, revealing their potential use as early markers for PD, that could contribute to both disease diagnosis and follow up of disease progression.

## REFERENCES

Aguirre GK, Detre JA, Zarahn E, Alsop DC (2002): Experimental design and the relative sensitivity of BOLD and perfusion fMRI. Neuroimage 15:488–500.

Andrade-Souza YM, Schwalb JM, Hamani C, Eltahawy H, Hoque T, Saint-Cyr J, Lozano AM (2008): Comparison of three methods of targeting the subthalamic nucleus for chronic stimulation in Parkinson's disease. Neurosurgery 62 Suppl 2: 875–883.

Aron AR, Poldrack RA (2006): Cortical and subcortical contributions to Stop signal response inhibition: Role of the subthalamic nucleus. J Neurosci 26:2424–2433.

Aron AR, Behrens TE, Smith S, Frank MJ, Poldrack RA (2007): Triangulating a cognitive control network using diffusion-weighted magnetic resonance imaging (MRI) and functional MRI. J Neurosci 27:3743–3752.

Ashburner J (2007): A fast diffeomorphic image registration algorithm. Neuroimage 38:95–113.

Auer DP (2008): Spontaneous low-frequency blood oxygenation level-dependent fluctuations and functional connectivity analysis of the 'resting' brain. Magn Reson Imaging 26:1055–1064.

Baudrexel S, Witte T, Seifried C, von Wegner F, Beissner F, Klein JC, Steinmetz H, Deichmann R, Roeper J, Hilker R (2011): Resting state fMRI reveals increased subthalamic nucleus-motor cortex connectivity in Parkinson's disease. Neuroimage 55: 1728–1738.

Biswal BB, Van Kylen J, Hyde JS (1997): Simultaneous assessment of flow and BOLD signals in resting-state functional connectivity maps. NMR Biomed 10:165–170.

Brunenberg EJ, Moeskops P, Backes WH, Pollo C, Cammoun L, Vilanova A, Janssen ML, Visser-Vandewalle VE, ter Haar Romeny BM, Thiran JP, Platel B (2012): Structural and resting state functional connectivity of the subthalamic nucleus: Identification of motor STN parts and the hyperdirect pathway. PLoS One 7:e39061.

Canteras NS, Shammah-Lagnado SJ, Silva BA, Ricardo JA (1990): Afferent connections of the subthalamic nucleus: A combined retrograde and anterograde horseradish peroxidase study in the rat. Brain Res 513:43–59.

Castle M, Aymerich MS, Sanchez-Escobar C, Gonzalo N, Obeso JA, Lanciego JL (2005): Thalamic innervation of the direct and indirect basal ganglia pathways in the rat: Ipsi- and contralateral projections. J Comp Neurol 483:143–153.

Cavanna AE, Trimble MR (2006): The precuneus: A review of its functional anatomy and behavioural correlates. Brain 129:564–583.

Chiken S, Nambu A (2014): Disrupting neuronal transmission: Mechanism of DBS? Front Syst Neurosci 8:33.

Clower DM, Dum RP, Strick PL (2005): Basal ganglia and cerebellar inputs to 'AIP'. Cereb Cortex 15:913–920.

Dagli MS, Ingeholm JE, Haxby JV (1999): Localization of cardiac-induced signal change in fMRI. Neuroimage 9:407–415.

Dai W, Varma G, Scheidegger R, Shankaranarayanan A, Schlaug G, Alsop D (2012): Measuring resting state functional networks using volumentric arterial spin labeling. Proc ISMRM Perfusion Workshop. Amsterdam.

DeCoteau WE, Thorn C, Gibson DJ, Courtemanche R, Mitra P, Kubota Y, Graybiel AM (2007): Learning-related coordination of striatal and hippocampal theta rhythms during acquisition of a procedural maze task. Proc Natl Acad Sci U S A 104:5644–5649.

Degos B, Deniau JM, Chavez M, Maurice N (2009): Chronic but not acute dopaminergic transmission interruption promotes a progressive increase in cortical beta frequency synchronization: Relationships to vigilance state and akinesia. Cereb Cortex 19: 1616–1630.

DeLong MR, Wichmann T (2007): Circuits and circuit disorders of the basal ganglia. Arch Neurol 64:20–24.

Detre JA, Leigh JS, Williams DS, Koretsky AP (1992): Perfusion imaging. Magn Reson Med 23:37–45.

Eickhoff SB, Stephan KE, Mohlberg H, Grefkes C, Fink GR, Amunts K, Zilles K (2005): A new SPM toolbox for combining probabilistic cytoarchitectonic maps and functional imaging data. Neuroimage 25:1325–1335.

Fernandez-Seara MA, Edlow BL, Hoang A, Wang J, Feinberg DA, Detre JA (2008): Minimizing acquisition time of arterial spin labeling at 3T. Magn Reson Med 59:1467–1471.

Fernandez-Seara MA, Aznarez-Sanado M, Mengual E, Loayza FR, Pastor MA (2009): Continuous performance of a novel motor sequence leads to highly correlated striatal and hippocampal perfusion increases. Neuroimage 47:1797–1808.

Fernandez-Seara MA, Aznarez-Sanado M, Mengual E, Irigoyen J, Heukamp F, Pastor MA (2011): Effects on resting cerebral blood flow and functional connectivity induced by metoclopramide: A perfusion MRI study in healthy volunteers. Br J Pharmacol 163:1639–1652.

Fernandez-Seara MA, Mengual E, Vidorreta M, Aznarez-Sanado M, Loayza FR, Villagra F, Irigoyen J, Pastor MA (2012): Cortical hypoperfusion in Parkinson's disease assessed using arterial spin labeled perfusion MRI. Neuroimage 59:2743–2750.

Fishman PS (2008): Paradoxical aspects of parkinsonian tremor. Mov Disord 23:168–173.

Folstein MF, Folstein SE, McHugh PR (1975): "Mini-mental state". A practical method for grading the cognitive state of patients for the clinician. J Psychiatr Res 12:189–198.

Forstmann BU, Keuken MC, Jahfari S, Bazin PL, Neumann J, Schafer A, Anwander A, Turner R (2012): Cortico-subthalamic white matter tract strength predicts interindividual efficacy in stopping a motor response. Neuroimage 60:370–375.

Goetz CG, Poewe W, Rascol O, Sampaio C, Stebbins GT, Counsell C, Giladi N, Holloway RG, Moore CG, Wenning GK, Yahr MD, Seidl L (2004): Movement Disorder Society Task Force report on the Hoehn and Yahr staging scale: Status and recommendations. Mov Disord 19:1020–1028.

Goetz CG, Tilley BC, Shaftman SR, Stebbins GT, Fahn S, Martinez-Martin P, Poewe W, Sampaio C, Stern MB, Dodel R, Dubois B, Holloway R, Jankovic J, Kulisevsky J, Lang AE, Lees A, Leurgans S, LeWitt PA, Nyenhuis D, Olanow CW, Rascol O, Schrag A, Teresi JA, van Hilten JJ, LaPelle N (2008): Movement Disorder Society-sponsored revision of the Unified Parkinson's Disease Rating Scale (MDS-UPDRS): Scale presentation and clinimetric testing results. Mov Disord 23: 2129–2170.

Goto M, Swanson LW (2004): Axonal projections from the parasubthalamic nucleus. J Comp Neurol 469:581–607.

Gradinaru V, Mogri M, Thompson KR, Henderson JM, Deisseroth K (2009): Optical deconstruction of parkinsonian neural circuitry. Science 324:354–359.

Hacker CD, Perlmutter JS, Criswell SR, Ances BM, Snyder AZ (2012): Resting state functional connectivity of the striatum in Parkinson's disease. Brain 135:3699–3711.

Hall EL, Robson SE, Morris PG, Brookes MJ (2014): The relationship between MEG and fMRI. Neuroimage 102:80–91.

Hammond C, Bergman H, Brown P (2007): Pathological synchronization in Parkinson's disease: Networks, models and treatments. Trends Neurosci 30:357–364.

Haynes WI, Haber SN (2013): The organization of prefrontal-subthalamic inputs in primates provides an anatomical

substrate for both functional specificity and integration: implications for basal ganglia models and deep brain stimulation. J Neurosci 33:4804–4814.

Helmich RC, Derikx LC, Bakker M, Scheeringa R, Bloem BR, Toni I (2010): Spatial remapping of cortico-striatal connectivity in Parkinson's disease. Cereb Cortex 20:1175–1186.

Helmich RC, Hallett M, Deuschl G, Toni I, Bloem BR (2012): Cerebral causes and consequences of parkinsonian resting tremor: A tale of two circuits? Brain 135:3206–3226.

Hirschmann J, Ozkurt TE, Butz M, Homburger M, Elben S, Hartmann CJ, Vesper J, Wojtecki L, Schnitzler A (2011): Distinct oscillatory STN-cortical loops revealed by simultaneous MEG and local field potential recordings in patients with Parkinson's disease. Neuroimage 55:1159–1168.

Hughes AJ, Daniel SE, Kilford L, Lees AJ (1992): Accuracy of clinical diagnosis of idiopathic Parkinson's disease: A clinico-pathological study of 100 cases. J Neurol Neurosurg Psychiatry 55:181–184.

Jubault T, Gagnon JF, Karama S, Ptito A, Lafontaine AL, Evans AC, Monchi O (2011): Patterns of cortical thickness and surface area in early Parkinson's disease. Neuroimage 55:462–467.

Kahan J, Urner M, Moran R, Flandin G, Marreiros A, Mancini L, White M, Thornton J, Yousry T, Zrinzo L, Hariz M, Limousin P, Friston K, Foltynie T (2014): Resting state functional MRI in Parkinson's disease: The impact of deep brain stimulation on 'effective' connectivity. Brain 137:1130–1144.

Kelly RM, Strick PL (2004): Macro-architecture of basal ganglia loops with the cerebral cortex: Use of rabies virus to reveal multisynaptic circuits. Prog Brain Res 143:449–459.

Kelly C, de Zubicaray G, Di Martino A, Copland DA, Reiss PT, Klein DF, Castellanos FX, Milham MP, McMahon K (2009): L-dopa modulates functional connectivity in striatal cognitive and motor networks: A double-blind placebo-controlled study. J Neurosci 29:7364–7378.

Keuken MC, Bazin PL, Crown L, Hootsmans J, Laufer A, Muller-Axt C, Sier R, van der Putten EJ, Schafer A, Turner R, Forstmann BU (2014): Quantifying inter-individual anatomical variability in the subcortex using 7 T structural MRI. Neuroimage 94:40–46.

Krack P, Poepping M, Weinert D, Schrader B, Deuschl G (2000): Thalamic, pallidal, or subthalamic surgery for Parkinson's disease? J Neurol 247 Suppl 2:II122–II134.

Krauth A, Blanc R, Poveda A, Jeanmonod D, Morel A, Szekely G (2010): A mean three-dimensional atlas of the human thalamus: Generation from multiple histological data. Neuroimage 49:2053–2062.

Kwak Y, Peltier S, Bohnen NI, Muller ML, Dayalu P, Seidler RD (2010): Altered resting state cortico-striatal connectivity in mild to moderate stage Parkinson's disease. Front Syst Neurosci 4: 143.

Lambert C, Zrinzo L, Nagy Z, Lutti A, Hariz M, Foltynie T, Draganski B, Ashburner J, Frackowiak R (2012): Confirmation of functional zones within the human subthalamic nucleus: Patterns of connectivity and sub-parcellation using diffusion weighted imaging. Neuroimage 60:83–94.

Lancaster JL, Woldorff MG, Parsons LM, Liotti M, Freitas CS, Rainey L, Kochunov PV, Nickerson D, Mikiten SA, Fox PT (2000): Automated Talairach atlas labels for functional brain mapping. Hum Brain Mapp 10:120–131.

Levesque JC, Parent A (2005): GABAergic interneurons in human subthalamic nucleus. Mov Disord 20:574–584.

Litvak V, Jha A, Eusebio A, Oostenveld R, Foltynie T, Limousin P, Zrinzo L, Hariz MI, Friston K, Brown P (2011): Resting oscillatory cortico-subthalamic connectivity in patients with Parkinson's disease. Brain 134:359–374.

Long D, Wang J, Xuan M, Gu Q, Xu X, Kong D, Zhang M (2012): Automatic classification of early Parkinson's disease with multi-modal MR imaging. PLoS One 7:e47714.

Luo C, Song W, Chen Q, Zheng Z, Chen K, Cao B, Yang J, Li J, Huang X, Gong Q, Shang HF (2014): Reduced functional connectivity in early-stage drug-naive Parkinson's disease: A resting-state fMRI study. Neurobiol Aging 35:431–441.

Magri C, Schridde U, Murayama Y, Panzeri S, Logothetis NK (2012): The amplitude and timing of the BOLD signal reflects the relationship between local field potential power at different frequencies. J Neurosci 32:1395–1407.

Marreiros AC, Cagnan H, Moran RJ, Friston KJ, Brown P (2013): Basal ganglia-cortical interactions in Parkinsonian patients. Neuroimage 66:301–310.

Massey LA, Yousry TA (2010): Anatomy of the substantia nigra and subthalamic nucleus on MR imaging. Neuroimaging Clin N Am 20:7–27.

Miyoshi E, Wietzikoski EC, Bortolanza M, Boschen SL, Canteras NS, Izquierdo I, Da Cunha C (2012): Both the dorsal hippocampus and the dorsolateral striatum are needed for rat navigation in the Morris water maze. Behav Brain Res 226:171–178.

Moran RJ, Mallet N, Litvak V, Dolan RJ, Magill PJ, Friston KJ, Brown P (2011): Alterations in brain connectivity underlying beta oscillations in Parkinsonism. PLoS Comput Biol 7: e1002124.

Nambu A, Tokuno H, Takada M (2002): Functional significance of the cortico-subthalamo-pallidal 'hyperdirect' pathway. Neurosci Res 43:111–117.

Odekerken VJ, van Laar T, Staal MJ, Mosch A, Hoffmann CF, Nijssen PC, Beute GN, van Vugt JP, Lenders MW, Contarino MF, Mink MS, Bour LJ, van den Munckhof P, Schmand BA, de Haan RJ, Schuurman PR, de Bie RM (2013): Subthalamic nucleus versus globus pallidus bilateral deep brain stimulation for advanced Parkinson's disease (NSTAPS study): A randomised controlled trial. Lancet Neurol 12:37–44.

Oldfield RC (1971): The assessment and analysis of handedness: The Edinburgh inventory. Neuropsychologia 9:97–113.

Pagonabarraga J, Corcuera-Solano I, Vives-Gilabert Y, Llebaria G, Garcia-Sanchez C, Pascual-Sedano B, Delfino M, Kulisevsky J, Gomez-Anson B (2013): Pattern of regional cortical thinning associated with cognitive deterioration in Parkinson's disease. PLoS One 8:e54980.

Pan WJ, Thompson GJ, Magnuson ME, Jaeger D, Keilholz S (2013): Infraslow LFP correlates to resting-state fMRI BOLD signals. Neuroimage 74:288–297.

Pereira JB, Junque C, Marti MJ, Ramirez-Ruiz B, Bargallo N, Tolosa E (2009): Neuroanatomical substrate of visuospatial and visuoperceptual impairment in Parkinson's disease. Mov Disord 24:1193–1199.

Petrides M (2012): The human cerebral cortex. An MRI atlas of the sulci and gyri in MNI stereotaxic space. Academic Press (Elsevier Inc.).

Postuma RB, Dagher A (2006): Basal ganglia functional connectivity based on a meta-analysis of 126 positron emission tomography and functional magnetic resonance imaging publications. Cereb Cortex 16:1508–1521.

Raichle ME (1998): Behind the scenes of functional brain imaging: A historical and physiological perspective. Proc Natl Acad Sci U S A 95:765–772.

Rico AJ, Barroso-Chinea P, Conte-Perales L, Roda E, Gomez-Bautista V, Gendive M, Obeso JA, Lanciego JL (2010): A direct projection from the subthalamic nucleus to the ventral thalamus in monkeys. Neurobiol Dis 39:381–392.

Robin X, Turck N, Hainard A, Tiberti N, Lisacek F, Sanchez JC, Muller M (2011): pROC: An open-source package for R and S+ to analyze and compare ROC curves. BMC Bioinformatics 12:77.

Seibert TM, Murphy EA, Kaestner EJ, Brewer JB (2012): Interregional correlations in Parkinson disease and Parkinson-related dementia with resting functional MR imaging. Radiology 263: 226–234.

Shimamoto SA, Ryapolova-Webb ES, Ostrem JL, Galifianakis NB, Miller KJ, Starr PA (2013): Subthalamic nucleus neurons are synchronized to primary motor cortex local field potentials in Parkinson's disease. J Neurosci 33:7220–7233.

Stoffers D, Bosboom JL, Deijen JB, Wolters E, Stam CJ, Berendse HW (2008a): Increased cortico-cortical functional connectivity in early-stage Parkinson's disease: An MEG study. Neuroimage 41:212–222.

Stoffers D, Bosboom JL, Wolters E, Stam CJ, Berendse HW (2008b): Dopaminergic modulation of cortico-cortical functional connectivity in Parkinson's disease: An MEG study. Exp Neurol 213:191–195.

Tang CC, Poston KL, Dhawan V, Eidelberg D (2010): Abnormalities in metabolic network activity precede the onset of motor symptoms in Parkinson's disease. J Neurosci 30:1049–1056.

Timmermann L, Florin E, Reck C (2007): Pathological cerebral oscillatory activity in Parkinson's disease: A critical review on methods, data and hypotheses. Expert Rev Med Devices 4:651–661.

Tomlinson CL, Stowe R, Patel S, Rick C, Gray R, Clarke CE (2010): Systematic review of levodopa dose equivalency reporting in Parkinson's disease. Mov Disord 25:2649–2653.

Vidorreta M, Wang Z, Detre JA, Fernandez-Seara MA (2012): Resting State Functional Connectivity of the Hand Motor Area Evaluated using Perfusion fMRI. Proc ISMRM Perfusion Workshop. Amsterdam.

Vidorreta M, Wang Z, Rodriguez I, Pastor MA, Detre JA, Fernandez-Seara MA (2013): Comparison of 2D and 3D single-shot ASL perfusion fMRI sequences. Neuroimage 66:662–671.

Vidorreta M, Benitez A, Pastor MA, Fernandez-Seara MA (2014): Reproducibility of resting state functional connectivity maps derived from ASL CBF data and concurrent BOLD. Proc ISMRM. Milan. p 1016.

Viviani R, Messina I, Walter M (2011): Resting state functional connectivity in perfusion imaging: Correlation maps with BOLD connectivity and resting state perfusion. PLoS One 6: e27050.

Volkmann J, Allert N, Voges J, Sturm V, Schnitzler A, Freund HJ (2004): Long-term results of bilateral pallidal stimulation in Parkinson's disease. Ann Neurol 55:871–875.

Wang J, Zhang Y, Wolf RL, Roc AC, Alsop DC, Detre JA (2005): Amplitude modulated continuous arterial spin labeling perfusion MR with single coil at 3.0 Tesla. Radiology 235:218–228.

Wang Z, Aguirre GK, Rao H, Wang J, Fernandez-Seara MA, Childress AR, Detre JA (2008): Empirical optimization of ASL data analysis using an ASL data processing toolbox: ASLtbx. Magn Reson Imaging 26:261–269.

Whitfield-Gabrieli S, Nieto-Castanon A (2012): Conn: A functional connectivity toolbox for correlated and anticorrelated brain networks. Brain Connect 2:125–141.

Williams DS, Detre JA, Leigh JS, Koretsky AP (1992): Magnetic resonance imaging of perfusion using spin inversion of arterial water.[erratum appears in Proc Natl Acad Sci U S A 1992 May 1;89(9):4220]. Proc Natl Acad Sci U S A 89:212–216.

Windischberger C, Langenberger H, Sycha T, Tschernko EM, Fuchsjager-Mayerl G, Schmetterer L, Moser E (2002): On the origin of respiratory artifacts in BOLD-EPI of the human brain. Magn Reson Imaging 20:575–582.

Woo CW, Krishnan A, Wager TD (2014): Cluster-extent based thresholding in fMRI analyses: Pitfalls and recommendations. Neuroimage 91:412–419.

Yelnik J (2002): Functional anatomy of the basal ganglia. Mov Disord 17 Suppl 3:S15–21.